

A Fully Spiking Hybrid Neural Network for Energy-Efficient Object Detection

Biswadeep Chakraborty, Xueyuan She, *Student Members, IEEE*, Saibal Mukhopadhyay, *Fellow, IEEE*

Abstract—This paper proposes a Fully Spiking Hybrid Neural Network (FSHNN) for energy-efficient and robust object detection in resource-constrained platforms. The network architecture is based on a Spiking Convolutional Neural Network using leaky-integrate-fire neuron models. The model combines unsupervised Spike Time-Dependent Plasticity (STDP) learning with backpropagation (STBP) learning methods and also uses Monte Carlo Dropout to get an estimate of the uncertainty error. FSHNN provides better accuracy compared to DNN based object detectors while being more energy-efficient. It also outperforms these object detectors, when subjected to noisy input data and less labeled training data with a lower uncertainty error.

Index Terms—Spiking Neural Networks, Leaky Integrate and Fire, Uncertainty Estimation, Generalization, Object Detection.

I. INTRODUCTION

Spiking Neural Networks (SNNs) are widely acclaimed as the third generation of neural networks given their low power consumption and close similarity in emulating how the brain works. There are two main aspects of spiking neural networks that make them attractive. Firstly, in SNNs, neurons communicate with each other through isolated, discrete electrical signals called spikes, as opposed to continuous signals, and work in continuous-time instead of discrete-time [1]. This spike-based inference methodology makes the spiking neural network energy-efficient[2]–[5]. In addition to this, spiking neural networks provides a novel unsupervised learning methodology using Spike Time Dependent Plasticity (STDP)[6]. STDP is a bio-plausible unsupervised learning mechanism that instantaneously manipulates the synaptic weights based on the temporal correlations between pre-and post-synaptic spike timings. STDP can also help improve robustness to noise in the inputs and assists in learning with less labeled data [7], [8]. These properties are attractive for real-world computer vision applications where the input can be imperfect and the labeled training data can be sparse.

The recent advances in Deep Neural Network-to-Spiking Neural Network (DNN-to-SNN) conversion mechanisms have enabled design of SNN with performance comparable to DNN in large datasets like ImageNet [9]. However, despite the recent developments, most of the existing works on spiking networks are primarily limited to classification. Many real-time autonomous applications such as lightweight drones and edge robots, where energy-efficient inference is crucial, have

This material is based on research supported by the Defense Advanced Research Projects Agency (DARPA) under contract number HR0011-17-2-0045. The views and conclusions contained herein are those of the authors and should not be interpreted as necessarily representing the official policies or endorsements, either expressed or implied, of DARPA.

B.Chakraborty, X.She and S. Mukhopadhyay are with the Department of Electrical and Computer Engineering, Georgia Institute of Technology, Atlanta, GA, 30332 USA e-mail:(biswadeep@gatech.edu; xshe@gatech.edu; saibal.mukhopadhyay@ece.gatech.edu)

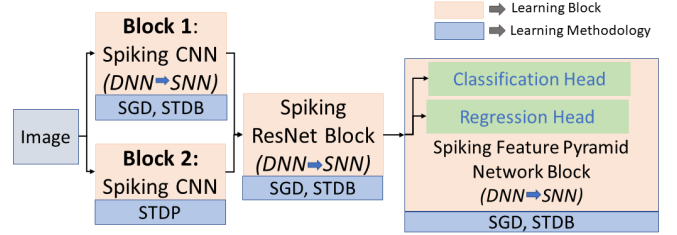


Fig. 1: General Block Diagram for Different Architectures

object detection as the primary task. Hence, an SNN for object detection will facilitate deployment of SNNs in such applications. Recent work on spiking based object detection [10] primarily uses the backpropagated SNN model and is trained on small networks (Tiny YOLO). This leads to a comparatively low accuracy compared to standard object detection networks. Moreover, the network does not use STDP learning limiting noise robustness or learning from less amount of labeled data.

In this paper, we propose a novel fully spiking neural network-based object detector using hybridization of unsupervised STDP based learning and supervised backpropagated learning. The proposed FSHNN network uses the baseline architecture of an object detection DNN, such as RetinaNet, as the backbone. The low-level feature space of the classifier is enhanced by fusing an auxiliary CNN block and a set of Spiking Convolution Layers pre-trained using STDP. Finally, we use a DNN-to-SNN conversion technique [11] while keeping the STDP-trained layer fixed to get the final object detector. The paper makes the following key contributions:

- We develop a fully spiking hybrid neural network for object detection integrating Stochastic Gradient Descent (SGD) and STDP based learning.
- We show that the STDP-based learning results in a more generalizable SNN model than a SGD-trained model.
- We adapt the Monte Carlo dropout methodology [12] to quantify uncertainty for FSHNN and use that to discriminate true positives from false-positive.
- We show that the hybridization of SGD-based and STDP-based learning within a SNN improves accuracy, improves generalizability, reduces uncertainty, and increases energy efficiency.

We evaluate the performance of FSHNN for object detection on MSCOCO dataset. Our experiments show that the FSHNN with six layers of STDP achieves an mAP of 0.426 compared to 0.388 achieved by the standard RetinaNet. We also show that FSHNN outperforms RetinaNet when tested with noisy input images and trained with limited labeled data. Using the Monte Carlo Dropout method, we further demonstrate that FSHNN based object detector has a lower uncertainty compared to RetinaNet. Also, we illustrate that the FSHNN

based object detector is more generalizable compared to the standard DNN based RetinaNet. Moreover, as the network uses spiking operations during inference, it naturally enhances the energy-efficiency of object detection.

The rest of the paper is structured as follows: Section II discusses the Related Works associated with this paper; Section III revolves around the architectures and baselines used in the evaluation; Section IV deals with the Experiments undertaken and the results obtained thereby; Section V summarizes the observations and discusses the conclusions we arrived at from the experiments.

II. RELATED WORKS

A. Object Detection:

Object detection has become a critical problem of many computer vision tasks as it requires the estimation of both the category to which an object belongs and its spatial location. Single-stage detection models like Single-shot multi-box detector (SSD) [13] and YOLO [14] achieve fast inference with the cost of lower mean Average Precision (mAP) and mean Average Recall (mAR). RetinaNet [15] overcomes these problems as it improves on the Faster-RCNN framework with the help of a focal loss and using ResNet+ Feature Pyramid Network (FPN) as the backbone network to extract features.

B. Spiking Object Detection:

Though object detection has been an important field of interest in computer vision, there is not much work for the use of spiking neural networks in object detection. Recently, Kim et al. implemented a spiking version of the YOLO object detection architecture [10]. They used channel-wise normalization and signed neurons with imbalanced thresholds to provide fast and accurate information transmission for deep SNNs. However, the proposed spiking YOLO object detector had a much lower performance than the standard DNN based YOLO and RetinaNet models.

C. DNN-to-SNN conversion:

Recent works have proposed weight normalization and threshold balancing methods to obtain minimal loss for accuracy during the conversion process. In this paper, we use the threshold balancing method [16] that gives near-lossless conversion performance for deep architectures like ResNet on complex Imagenet dataset.

Diehl et al. used the relationship between dynamics of the spiking neuron and the ReLU activation function for a fast DNN-to-SNN conversion [17], achieving a nearly lossless conversion on the MNIST dataset using parameter normalization.

Rueckauer et al. proposed the SNNToolbox framework [18] which improved the SNN scores after conversion. Miquel et al. used the algorithm and implementations suggested by Rueckauer et al. for a DNN-to-SNN conversion of the RetinaNet [19]. In this paper, we use the Spiking-RetinaNet implementation done by Miquel et al. as the initialization step. We use a rate-based encoding scheme for the DNN-to-SNN conversion process i.e. the neurons generate spike-trains whose rate approximates the analog activation corresponding to the original DNN. This encoding becomes more accurate as the simulation duration is increased entailing a higher resolution at the price of scaling up the computational cost.

D. STDP based Unsupervised learning in SNN

Spike Timing Dependent Plasticity (STDP) [20] is a variant of the Hebbian unsupervised learning algorithm. STDP describes the changes of a synaptic weight according to the relative timing of pre and post-synaptic spikes. In STDP, if a presynaptic spike precedes a post-synaptic one, a synaptic weight is potentiated.

There are various spiking neural networks (SNNs) to solve object recognition and image classification tasks by converting the traditional DNNs into spiking networks by replacing each DNN computing unit with a spiking neuron [21]. Kheradpisheh et al. proposed a STDP based spiking deep convolutional neural network for object recognition [22]. Wu et al. similarly proposed a spatio-temporal backpropagation for training Spiking Neural Networks [23]. This type of spiking neural networks primarily aim to reduce the energy consumption in DNNs while achieving a similar accuracy.

E. Back-propagation based Supervised Learning in SNN

Backpropagation-based supervised learning for spiking neural networks has played a critical role in improving their performance. Rathi et. al used a hybrid training technique that combines ANN-SNN conversion and spike-based BP that reduces the latency and helps in better convergence [11]. The authors used the ANN-SNN conversion as an initialization step followed by spike-based backpropagation (STDB) incremental training. The authors also demonstrated the approach of taking a converted SNN and incrementally training it using backpropagation. This hybrid approach improves the energy-efficiency and accuracy compared to standard models trained with either only spike-based backpropagation or only converted weights.

F. Generalizability of Neural Networks

Recent works [24]–[26] have analyzed overparameterized (wide) neural networks from a theoretical perspective by connecting them to reproducing kernel Hilbert spaces. The papers have also shown that under proper conditions, the weights of a well-trained overparameterized network remain very close to their initialization. Thus, during training the model searches within some class of reproducing kernel functions, where the associated kernel is called the “neural tangent kernel” which only depends on the initialization of the weights.

Another line of research has worked on comparing the generalization error while using different training strategies [27]. The authors show that we can control the generalization error of a training algorithm using the Hausdorff dimension of its trajectories. Gurbuzbalaban et al. showed that depending on the structure of the Hessian of the loss at the minimum, and the choices of the algorithm parameters η, b , the SGD iterates will converge to a heavy-tailed stationary distribution [28].

Recent works have worked on determining the generalization characteristics of the object proposal generation that is the first step in detection models [29]. A more generalizable object proposal can help to scale detection models to a larger number of classes with fewer annotations. Thus, the paper studies how a detection model trained on a small set of source classes can provide proposals that generalize to unseen classes.

III. MOTIVATION

In this section, we discuss the primary motivations for using a hybrid spiking neural network-based object detector. We discuss the generalization advantages we can obtain by fusing features learned using STDP with the SGD process.

A. LIF and STDP Dynamics

Spiking neural network uses biologically plausible neuron and synapse models that can exploit temporal relationship between spiking events [30],[31]. There are different models that are developed to capture the firing pattern of real biological neurons. We choose to use Leaky Integrate Fire (LIF) model in this work described by:

$$\tau_m \frac{dv}{dt} = -v(t) + RI(t) \quad (1)$$

$$v = v_{\text{reset}}, \text{ if } v > v_{\text{threshold}} \quad (2)$$

where, v , the membrane potential, and τ_m , the membrane time constant of the neuron. R is the resistance of the integrate-and-fire model and $I(t)$ is the sum of the current signal from all synapses that connect to the neuron. In SNN, two neurons connected by one synapse are referred to as pre-synaptic neurons and post-synaptic neurons. Conductance of the synapse determines how strongly two neurons are connected and learning is achieved through modulating the conductance using STDP [32], [33]. With two operations of STDP, namely, long-term potentiation (LTP) and long-term depression (LTD), SNN can extract the causality between spikes of two connected neurons from their temporal relationship. More specifically, LTP is triggered when post-synaptic neuron spikes closely after a pre-synaptic neuron spike, indicating a causal relationship between the two events. On the other hand, when a post-synaptic neuron spikes before pre-synaptic spike arrives or without receiving a pre-synaptic spike at all, the synapse goes through LTD.

In a STDP model, the change in synaptic weight induced by the pre-and post-synaptic spikes at times t_{pre}, t_{post} are defined by:

$$\Delta W_{ij} = \begin{cases} a_{LTP} (W_{ij} - W_{LB}) (W_{UP} - W_{ij}) & t_j - t_i \leq 0, \\ a_{LTD} (W_{ij} - W_{LB}) (W_{UP} - W_{ij}) & t_j - t_i > 0, \end{cases} \quad (3)$$

where i and j refer to the post- and pre-synaptic neurons, respectively, Δw_{ij} is the amount of weight change for the synapse connecting the two neurons, and a_{LTP} , and a_{LTD} scale the magnitude of weight change. Besides, $(W_{ij} - W_{LB}) \times (W_{UP} - W_{ij})$ is a stabilizer term which slows down the weight change when the synaptic weight is close to the weight's lower (W_{LB}) and upper (W_{UB}) bounds.

B. Transfer Learning and Feature Fusion

In this subsection, we motivate the feature fusion of STDP and SGD processes for object detection. We argue that features learned using STDP can complement the standard SGD making the training simpler, more generalizable, and robust. Zeiler et. al. observed that the lower layers of a DNN converged much faster compared to the higher layers [34]. They also showed that small transformations in the input image impact the lower layers more than the higher layers. Donahue et al. have

empirically demonstrated that a convolutional network trained on a large dataset can be successfully generalized to other tasks where less data is available [35]. These observations motivated us to use additional layers in the initial stages of the backbone classifier to capture the low-level features. Yosinski et al. showed that lower level features can be transferred to different networks to get superior performance [36]. Developing on these ideas, we utilize the spiking convolutional layers trained using the unsupervised STDP method since it can better apprehend local features compared to the standard DNN.

Thus, we show the generalizability of STDP compared to SGD that would subsequently motivate us to demonstrate the generalization of spiking neural network models.

C. Generalizability of STDP

In this subsection, we compare the generalization bounds of a spiking convolutional neural network to its DNN counterpart with the same architecture. Jacot et al. showed that the generalizability of an infinitely wide neural network is dependent on the initialization where a better initialization improves the generalizability of the network [24].

Simsekli et al. demonstrated that the generalization error is controlled by the uniform Hausdorff dimension of the learning algorithm, with the constants inherited from the regularity conditions [27]. The authors further showed that the Hausdorff dimension is controlled by the tail behavior of the process, with heavier tails implying less generalization error. Therefore, we study the tail indices of the trajectories of the STDP and SGD learning methodologies as a measure of its Hausdorff Dimension.

Recent literature has shown that the STDP based learning in SNN follows an Ornstein-Uhlenbeck (OU) process [37]. On the other hand, SGD follows a Feller process [38]. So, we compare the tail indices of the two stochastic processes to study their heavy-tailed natures.

We use stochastic differential equations (SDEs) to formulate local plasticity rules for parameters θ_i that control synaptic connections (if $\theta_i > 0$) and synaptic weights $w_i = \exp(\theta_i - \theta_0)$

$$d\theta_i = \left(b \frac{\partial}{\partial \theta_i} \log p^*(\theta) \right) dt + \sqrt{2Tb} \cdot d\mathcal{W}_i$$

where $d\mathcal{W}_i$ denotes an infinitesimal (4)

step of a random walk (Wiener process), drift diffusion $b =$ learning rate, $T =$ temperature ($T=1$ until last slide)

The Fokker-Planck (FP) equation tracks the resulting evolution of the SNN configurations θ over time, yielding the stationary distribution $\frac{1}{z} p^*(\theta)^{1/T}$ which follows the Ornstein-Uhlenbeck process [37]

$$\begin{aligned} \frac{\partial}{\partial t} p_{FP}(\theta, t) = \sum_i - \frac{\partial}{\partial \theta_i} \left(\left(b \frac{\partial}{\partial \theta_i} \log p^*(\theta) \right) p_{FP}(\theta, t) \right) \\ + \frac{\partial^2}{\partial \theta_i^2} (Tb p_{FP}(\theta, t)) \end{aligned} \quad (5)$$

The practically relevant forms of the target distribution $p^*(\theta)$ of network configurations depend on the type of learning. For this case, we consider the unsupervised learning

TABLE I: Table showing the hyperparameters used for the LIF and the STDP models

STDP Parameters	Value	LIF Parameters	Value
LTP Learning Rate (a_{LTP})	0.004	R	1
LTD Learning Rate (a_{LTD})	0.003	τ_m	10
W_{LB}	0	$\mathbf{v}_{\text{threshold}}$	-40
W_{UP}	1	$\mathbf{v}_{\text{reset}}$	-80

method described in [39]. We perform a tail index analysis of STDP in deep SNN, similar to the method adopted in [40].

Several works have explored estimation of the tail-index of an extreme-value distribution [41], [42]. However, most of these methods fail to estimate the tail index of α -stable distributions [43], [44]. We consider the estimation method proposed by Mohammadi et. al. [45] which has a faster convergence rate and smaller asymptotic variance than the aforementioned methods. The basic approach is discussed below.

In the following, $f_X(\cdot)$ and $F_X(\cdot)$ denote the probability density function and distribution function of a random variable X , respectively, and ξ_p^X satisfies $p = P(X \leq \xi_p^X)$.

We know for the one-dimensional case, if X_1, \dots, X_n be a sequence of i.i.d. random variables with probability density function $f_X(\cdot)$, and $X_{1:n} \leq \dots \leq X_{n:n}$, $\frac{j}{n} \rightarrow p \in (0, 1)$, then

$$\lim_{n \rightarrow +\infty} \sqrt{n} (X_{j:n} - \xi_p^X) \rightarrow_D N \left(0, \frac{p(1-p)}{(f_X(\xi_p^X))^2} \right) \quad (6)$$

where " \rightarrow_D " denotes convergence in distribution.

We consider $|X|_{1:n} \leq \dots \leq |X|_{n:n}$ such that $|x| = \left(\sum_{k=1}^{\lambda} x_k^2 \right)^{1/2} \forall x = (x_1, \dots, x_d) \in \mathbb{R}^d$. Consider an i.i.d. sequence of strictly α -stable random vectors $\mathbf{X}_i, i = 1, 2, \dots, m$ with dimension $d \geq 1$. Let $\mathbf{Y} = \sum_{i=1}^m \mathbf{X}_i$. As Mohammadi et. al. has shown [45],

$$\left(\xi_p^{\log|Y|} - \xi_p^{\log|X_1|} \right) / \log m = 1/\alpha$$

These relations were used to construct an estimator for $1/\alpha$ as follows:

Let $\{X_i\}_{i=1}^K$ be a collection of random variables with $X_i \sim S\alpha S(\sigma)$ and $K = K_1 \times K_2$. Define $Y_i \triangleq \sum_{j=1}^{K_1} X_{j+(i-1)K_1}$ for $i \in [1, K_2]$. Then, the estimator

$$\hat{\frac{1}{\alpha}} \triangleq \frac{1}{\log K_1} \left(\frac{1}{K_2} \sum_{i=1}^{K_2} \log |Y_i| - \frac{1}{K} \sum_{i=1}^K \log |X_i| \right) \quad (7)$$

converges to $1/\alpha$ almost surely, as $K_2 \rightarrow \infty$.

In order to estimate the tail-index α at iteration k , we first partition the set of data points $\mathcal{D} \triangleq \{1, \dots, n\}$ into many disjoint sets $\Omega_k^i \subset \mathcal{D}$ of size b , such that the union of these subsets give all the data points. Formally, for all $i, j = 1, \dots, n/b, |\Omega_k^i| = b, \cup_i \Omega_k^i = \mathcal{D}$, and $\Omega_k^i \cap \Omega_k^j = \emptyset$ for $i \neq j$. We then compute the full gradient $\nabla f(\mathbf{w}_k)$ and the stochastic gradients $\nabla \tilde{f}_{\Omega_k^i}(\mathbf{w}_k)$ for each minibatch Ω_k^i . Finally, we compute the stochastic gradient noises $U_k^i(\mathbf{w}_k) = \nabla \tilde{f}_{\Omega_k^i}(\mathbf{w}_k) - \nabla f(\mathbf{w}_k)$, vectorize each $U_k^i(\mathbf{w}_k)$ and concatenate them to obtain a single vector, and compute the reciprocal of the estimator given in Eq. 7. We use $K = pn/b$ and K_1 is the divisor of K that is the closest to \sqrt{K} for our experiments.

Similar to the analysis done by Simsekli et. al, we evaluate

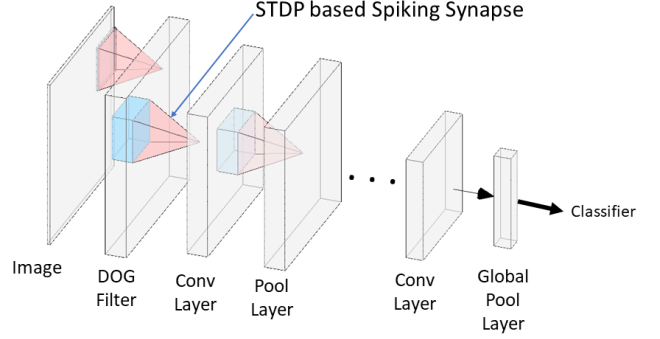


Fig. 2: Architecture used for tail index analysis

TABLE II: Comparison of Tail Indices α of SGD, STDP for varying depth in Convolutional Networks[40]

No. of Conv. Layers	SGD	STDP
3	1.297	1.206
4	1.291	1.193
5	1.284	1.188
6	1.273	1.181

the tail-index of the standard CNN trained with the SGD and the spiking convolutional neural networks trained with STDP processes [40]. The generalized architecture model used for this experiments are shown in Fig. 2. For the spiking convolution layers, we use STDP based learning method as described in Fig. 2 similar to the training methodology proposed by Kheradpisheh et al. [22][46]. The parameters used for the simulation are enlisted in Table I. It is to be noted that this training is completely unsupervised until the final global pooling and classifier which are trained with the labels are given. We used a deep SNN, comprising several convolutional, trained using STDP, and pooling layers. For the SGD based DNN approach, we use the same architecture as described in Fig. 2, but used standard Convolutional Neural Networks (CNNs) instead and trained the network using SGD on a cross-entropy loss function. The SGD was trained with a batch size of 32, a learning rate of 0.004, and a momentum of 0.9. Both the networks were trained for 300 epochs before their tail indices were estimated. The experiment is repeated with varying numbers of layers and is evaluated on the MNIST dataset and the tail indices are reported in Table II. We observe that the STDP process has a smaller value of α for each of the cases thus implying that the distribution has a heavier tail and thus is more generalizable.

IV. PROPOSED ARCHITECTURE

In this section, we introduce the novel Fully Spiking Hybrid Neural Network-based Object Detector. Since fusion improves the learning ability of low-level features and STDP is more generalizable than SGD, we introduce a model that fuses the STDP and the SGD based learning methods.

A. Image to Spike Conversion and Output Decoding

SNNs process Poisson rate-coded input spike trains, wherein, each pixel in an image is converted to a Poisson-distribution-based spike train with the spiking frequency pro-

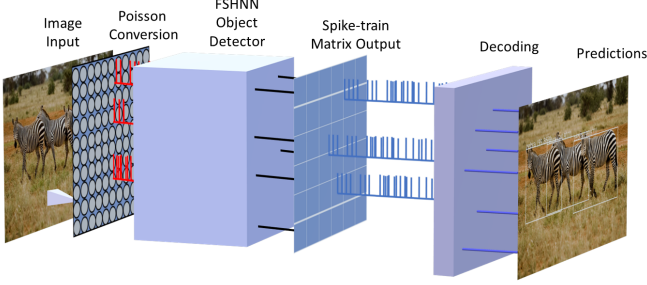


Fig. 3: Illustrative scheme of the FSHNN simulation for a specific time window

portional to the pixel value. As shown in Fig 3, the input layer consists of a single neuron per image pixel. Each input is a Poisson spike-train, which is fed to the excitatory neurons of the second layer. The rates of spikes of each neuron are proportional to the intensity of the corresponding pixel. The intensity values of the image are converted to Poisson-spike with firing rates proportional to the intensity of the corresponding pixel. The obtained spiking object detector is exposed to the input image within a given time window where the image is fed to the model as a matrix of constant currents as shown in Fig. 3. It then propagates through the network driving the final layer to a steady spiking rate. After these rate values are denormalized they can be processed and decoded.

Decoding: The decoding is performed in the same way as the original ANN output activations, in post-processing, by selecting the output neuron with the largest number of spikes. In order to facilitate the success of this decoding rule, in the training phase, the postsynaptic neuron corresponding to the correct label is assigned a desired output spike train, while a zero output is assigned to the other postsynaptic neurons.

However for the object detection problem, the regression problem to determine the bounding boxes poses a challenge as it requires high numerical precision. Low firing rate in neurons and lack of an efficient implementation method of leaky-ReLU in SNNs often leads to a performance degradation for such high-precision tasks as shown by Kim et al. [10]. Hence, as shown by the authors, we used a fine-grained channel-wise normalization to enable fast and efficient information transmission in deep SNNs. This normalizes the weights by the maximum possible activation in a channel-wise manner instead of the conventional layer-wise manner. Channel-norm normalizes extremely small activations such that the neurons can transmit information accurately in a short period of time. These small activations are critical in regression problems and significantly affect the model’s accuracy. The output decoding is thus done by accumulating the V_{mem} to decode the spike trains from the regression and classification heads

B. Fully Spiking Hybrid Object Detector Architecture

For the FSHNN based Object Detector model, we take the DNN based RetinaNet model[15] with a backbone network of ResNet 101. We augment the ResNet layers with an Auxiliary CNN block and an STDP block as shown in Fig. 1. We keep the STDP block frozen and convert the rest of the DNN to a

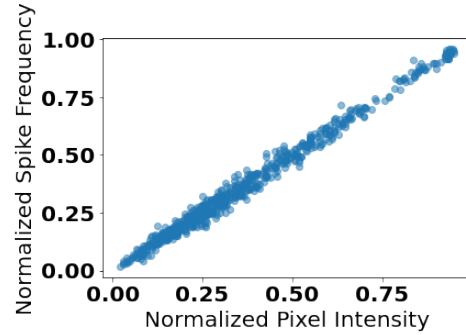


Fig. 4: Plot for the Normalized Spike Frequency vs the Normalized Pixel Intensity

Spiking network using a DNN to SNN conversion method as described in [11]. Hence, we get a fully spiking object detector with augmented STDP layers and an auxiliary CNN block in the backbone. The motivation for such a model is to compare the benefits of adding an unsupervised training methodology in the object detection network.

For this paper, we use a ResNet-101 as the backbone network. For **Block 1** in FSHNN, we use four convolutional layers converted from their DNN counterparts. **Block 2** for FSHNN is composed of the STDP layers. As we repeat the experiments with multiple STDP layers, we keep on increasing a 64×64 filter in each case at the end of the last Spiking Convolutional Layer in **Block 2** as shown in Fig 1. The detailed filter sizes for the **Blocks 1,2** and the ResNet are given in Fig 5. However, it is to be noted that the **STDP SCNN module** shown in Fig. 5 is a general representation for the STDP block with varying Spiking Convolutional layers trained using STDP. We perform experiments by varying the number of Spiking Convolutional layers from 3 to 6.

C. STDP based Spiking CNN architecture

The architecture of the unsupervised STDP based convolutional module is shown in Fig. 6. The architecture differs from the conventional DNN based architectures in the following respects.

The connections are made with plastic synapses following the STDP learning rule. When the neuron in the SCNN layer spikes, an inhibitory signal is sent to the neurons at the same spatial coordinates across all depths in the same layer. This inhibition facilitates the neurons at the same location to learn different features and thus, achieves a competitive local learning behavior of robust low-level features. Another problem in multi-layered SNNs is that a spiking neuron needs several spikes to emit a single spike that leads to diminishing spiking frequency [47]. To tackle this problem, we use a layer-wise learning procedure where after learning the first layer is complete, its cross-depth inhibition is disabled while keeping its conductance matrix fixed. Hence, the spiking threshold for the neurons in the first layer is lowered to provide a higher spiking frequency. In this way, the neurons in the first layer receive input from the images and produce spikes that in turn facilitate the learning in the second layer and so on.

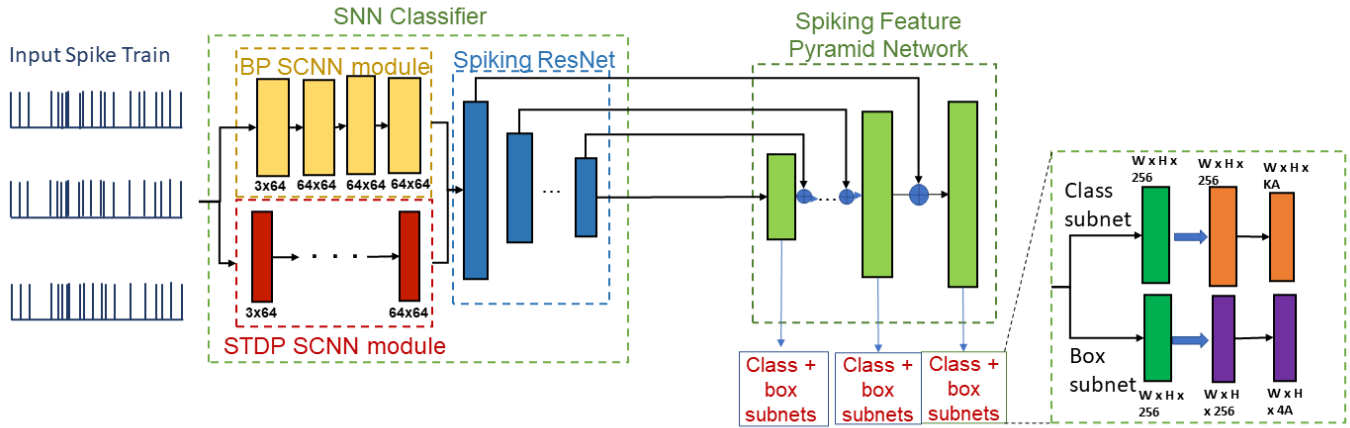


Fig. 5: Architectural block diagram showing the different parts of the FSHNN spike based object detector with varying STDP layers

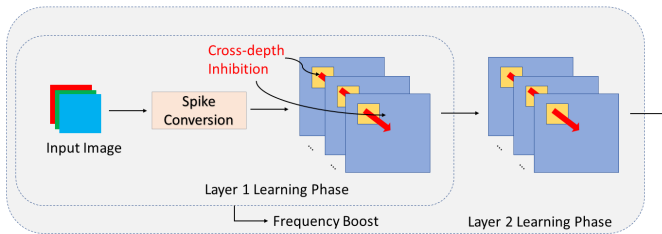


Fig. 6: The architecture of the spiking convolutional module for feature extraction and layer-by-layer learning process

D. Learning Methodology

The learning methodology of the FSHNN is done in the following five-step process which is summarized in Fig. 7.

- We train the STDP block independently as a separate neural network as shown in Fig 6 on the ImageNet traffic dataset. The ImageNet traffic dataset is a subset of the ImageNet dataset consisting of only the traffic signs, cars, and pedestrians. Since STDP is an unsupervised learning method, it need not be trained on the full ImageNet dataset. This is motivated by the observations shown by Kheradpisheh et al. [22].
- We use these pre-trained STDP layers as a supplement to the ResNet backbone as described above.
- With these STDP layers frozen in place, we use the DNN-to-SNN conversion process using the process described by Miquel et al[19].
- For the DNN-to-SNN conversion, we use a rate-encoding of the activations. For the conversion process, we assume the firing rate of the spiking neurons over a certain time window approximates the activations of the original ana-

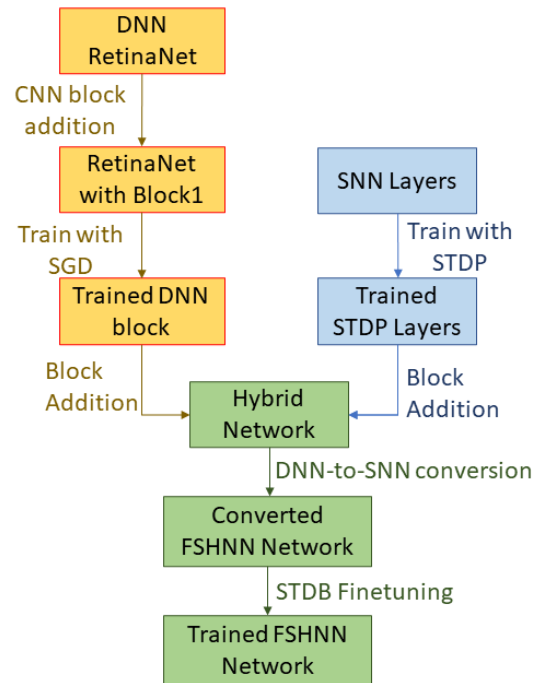


Fig. 7: Flowchart Showing the Learning Methodology of the FSHNN Network

TABLE III: Table showing the hyperparameters used for the SNN training process

Parameter	Value	Parameter	Value
<i>Batch Size</i>	32	<i>Parameter α for STDB</i>	0.3
<i>Momentum parameter for the SGD optimizer</i>	0.95	<i>Parameter β for STDB</i>	0.01
<i>Epochs</i>	300	<i>Weight Decay parameter for the optimizer</i>	0.0005
<i>Timesteps</i>	350	<i>Optimizer for SNN Backpropagation</i>	SGD

log neurons [48] and there is a one-to-one correspondence between the analog and spiking neurons. The dynamics of the spiking neurons are modeled using the Leaky Integrate and Fire (LIF) model.

- After this conversion is done, we retrain the model with the Spike Time Dependent Backpropagation (STDB) method to finetune the weights and activations obtained. Table III. shows the implementation details of the spiking neural network STDB training method.

It is to be noted here that, in this paper we use the Focal Loss [15], which addresses the imbalance between the trivial but over-represented background class and the object classes. Focal loss (FL) uses a modulating factor $(1 - p_t)^\gamma$ to the cross entropy loss, with tunable focusing parameter $\gamma \geq 0$ and is defined as:

$$FL(p_t) = -(1 - p_t)^\gamma \log(p_t) \quad (8)$$

The parameters of the LIF and the STDP dynamics used in this paper are summarized in Table II.

Hence, using the weights obtained as an initialization point, we retrain these other supervised spiking layers using the Spike Time Dependent Backpropagation (STDB) process [11]. STDB is a hybrid training methodology that takes the converted SNN and uses its weights and thresholds as an initialization step for spike-based backpropagation. It then performs incremental spike-timing dependent backpropagation (STDB) on this initialized network to obtain an SNN that converges within few epochs and requires fewer time steps for input processing. STDB is performed with a novel surrogate gradient function defined using the neuron’s spike time. Thus, using the DNN-to-SNN conversion, STDP based training of SCNN layers, and STDB fine-tuning, we get a fully spiking RetinaNet object detector.

E. Model Uncertainty in Spiking Object Detectors

1) Monte Carlo Dropout for Spiking Neural Networks

Recent work has shown that the use of dropout during training can be used as an approximation of the Monte Carlo simulation, thus giving us an estimate of the Bayesian inference done on the network [49]. Lee et al [50] introduced the dropout technique for spiking networks, though they used it only during training and not for inference. In this paper, we use the dropout during both training and inference so that inference with dropout enabled can be interpreted as an approximate Bayesian Inference in deep Gaussian processes, similar to its DNN counterpart.

The dropout method in SNNs differs from that in the standard DNNs where each epoch of training has several iterations of mini-batches and during each iteration, randomly selected units are disconnected from the network while weighting by

its posterior probability. On the other hand, in SNNs, each iteration has more than one forward propagation depending on the time length of the spike train. Thus, the output error is back-propagated and the network parameters are modified only at the last time step. Also, during training, the set of connected units within an iteration of mini-batch data remains the same in such a way that the same random subset of units constitutes the neural network during each forward propagation within a single iteration. Similarly, during inference also, we take a random subset of the entire network in a single iteration and each iteration has multiple forward passes. Thus, we use multiple such forward samples and partition the individual detections into observations as discussed in [51] to obtain the label uncertainty and the spatial bounding box uncertainty estimates.

2) Epistemic Uncertainty Estimation for Object Detectors

Object Detection is concerned with estimating a bounding box alongside a label distribution for multiple objects in a scene. We extend the concept of Dropout Sampling as a means to perform tractable variational inference from image recognition to object detection. We employ the dropout sampling approximation method as described in [49] to sample from the distribution of weights $p(\mathbf{W} | \mathbf{T})$ where \mathbf{W} are the learned weights of the FSHNN detection network and \mathbf{T} is the training data. We apply MC Dropout treating the object detector as a black box [51]. Uncertainty is then estimated as sample statistics from spatially correlated detector outputs.

In the object detectors, we use the dropout layers after each of the convolution layers in the main ResNet block in the backbone network. This modified network is trained with the dropout layers as discussed above. With these trained layers, we use the dropout during inference which acts as a Monte Carlo Sampling technique. Every forward pass through the network corresponds to performing inference with a different network $\tilde{\mathbf{W}}$ which is approximately sampled from $p(\mathbf{W}|\mathbf{T})$.

V. EXPERIMENTAL RESULTS

In this section, we present experimental results to evaluate the performance of FSHNN. First, we evaluate the performance of FSHNN on the MS-COCO dataset [52]. The MS COCO dataset has 223K frames with instances from 81 different object categories, and a training/testing split of 118K/5K. Second, we evaluate the performance of FSHNN considering varying input noise levels and training the models on limited labeled data. Third, we compare FSHNN to other spiking and non-spiking object detectors trained using backpropagation considering object detection performance and energy efficiency. Finally, we also show that the object proposal of the FSHNN based object detector generalizes better for unseen data classes in comparison to the standard object detectors like RetinaNet.

All the simulations were done on a computer with Intel Core i7-8700K CPU @ 3.70GHz CPU and 16GB NVIDIA GeForce GTX1080Ti GPU. RetinaNet trained from scratch and FSHNN trained with hybrid conversion-and-STDB are evaluated for 100-time steps. One epoch of training (inference) of the RetinaNet takes 79 (0.02) minutes and 8.67 (2.25) GB of GPU memory. On the other hand, one epoch of SNN training

(inference) takes 125 (23.47) minutes and 15.36 (2.41) GB of GPU memory for the same hardware and batch size of 32. We evaluate the performance of the FSHNN based object detector trained for the MS-COCO dataset.

The hyperparameters of the SNN used for the experiments are shown in Table III and that of the LIF dynamics in Table I.

The remainder of this section is organized as follows:

- (A) **Evaluation Metrics:** Here we define the metrics used for the evaluation of the different models described
- (B) **Performance Evaluation of FSHNN:** Here we evaluate the performance of the FSHNN models. To test the robustness of the model, we further experiment with the following adversarial conditions:
 - *Performance with Input Noise in Testing Images:* We evaluate the performance of the FSHNN object detector after adding different levels of Gaussian white noise to the images.
 - *Performance after Training with Less Labeled Data:* To further evaluate the performance of the FSHNN model, we re-train it with decreasing amount of labeled data and evaluated its performance.
- (C) **Comparison with Baselines:** We compare the performance of the proposed FSHNN model with some baseline object detector models. This comparison is further divided into two parts:
 - *Performance Comparison:* We compare the performance of the FSHNN based object detector with the other baselines.
 - *Generalizability of Object Proposals:* We perform empirical analysis to test the generalizability of the object proposal between the FSHNN and the other baselines
- (D) **Comparison with other Hybrid Models:** We compared the performance and generalizability of the FSHNN model for other DNN-based Hybrid object detection models
- (E) **Ablation Studies:** We performed some ablation studies to study the significance of the addition of the STDP and the backpropagation blocks to the Spiking RetinaNet model
- (F) **Energy Efficiency Comparison:** We performed an energy efficiency of the SNN based FSHNN object detector in comparison to DNN based object detection models.
- (G) **Comparison to Spiking Yolo:** We also performed an empirical comparison of the FSHNN based object detector with the Spiking YOLO model [10].

A. Evaluation Metrics

The two main evaluation metrics used to quantify the performance of object detectors discussed above are:

- *Mean Average Precision (mAP)* : mAP is a metric for evaluating object detection performance. mAP measures a detector’s ability to detect all objects in a closed set dataset with a correct classification and accurate localization ($\text{IoU} \geq 0.5$), while minimizing incorrect detections and their confidence score. For performance on the detection task, we use the Mean Average Precision

(mAP) at 0.5 IOU. The maximum mean average precision achievable by a detector is 100%. The mAP can be divided into three subclasses to depict the average precision of small object detection AP_S , medium object detection AP_M and large object detection AP_L depending on the size of the ground truth object.

- *Mean Average Recall (mAR)* : Another metric for evaluating the performance of an object detector is the mean Average Recall (mAR). While precision is defined by the ratio of the true positives to the sum of true positives and false positives, recall is defined as the ratio of the number of true positives to the number of ground truths. Thus, the Average Recall is defined as the recall averaged over all $\text{IoU} \in [0.5, 1.0]$ and can be computed as twice the area under the recall-IoU curve. It should be noted that for the evaluation on MS-COCO, distinctions are made among different classes and its AR metric is calculated on a per-class basis, just like AP.
- *Uncertainty Error (UE)* [53]: This metric represents the ability of an uncertainty measure to accept correct detection and reject incorrect detection. The uncertainty error is the probability that detection is incorrectly accepted or rejected at a given uncertainty threshold. We use the Minimum Uncertainty Error (MUE) at 0.5 IOU to determine the ability of the detector’s estimated uncertainty to discriminate true positives from false positives. The lowest MUE achievable by a detector is 0%. We define the Categorical MUE (CMUE) since we are using the Categorical entropy and finally, we average the CMUE overall categories in a testing dataset to derive the Mean (Categorical) MUE (mCMUE).

B. Performance Evaluation of FSHNN

In this section, we evaluate the performance of the FSHNN based object detector on the MS-COCO dataset. We do so by performing three separate experiments. First, we evaluate the performance of the model under normal circumstances, train with all the input data, and test with clean images. We repeat this experiment for multiple STDP layers in the **Block 2**, as shown in Fig. 1. The results are summarized in Table IV. Fig. 9 demonstrates the performance of the FSHNN object detector for a clean and noisy input image.

We see that the insertion of more STDP layers reduces both classification and regression losses, but the classification loss reduces more. Also, from Fig. 8, we see that the inclusion of the STDP layers increases the AP for all small, medium, and large object detections.

1) Performance with Input Noise in Testing

We evaluate the average precision and recall of the proposed FSHNN based object detector on the MS-COCO dataset under the signal-to-noise ratios (S.N.R) of 30dB and 15dB. We use a standard additive white Gaussian noise for these experiments. The results of the experiments are summarized in Table V. We see an increment of 12% on the addition of 3 new STDP layers for the no noise case. The addition of STDP layers plays a more significant role as the network is subjected to more adversarial conditions for example when there is an increase in the input noise level or the network is trained with a lesser

TABLE IV: Table showing Performance of the FSHNN based Object Detector with Increasing STDP Layers

Number of STDP Layers	Classification Loss	Regression Loss	mAP	AP _S	AP _M	AP _L	mAR	AR _S	AR _M	AR _L	mCMUE
3	0.4127	0.6912	0.379	0.198	0.407	0.482	0.492	0.292	0.554	0.615	0.251
4	0.3841	0.6787	0.392	0.203	0.425	0.507	0.515	0.308	0.578	0.635	0.244
5	0.3352	0.6536	0.409	0.211	0.439	0.518	0.527	0.316	0.591	0.652	0.236
6	0.3076	0.6193	0.426	0.229	0.452	0.533	0.541	0.327	0.612	0.668	0.229

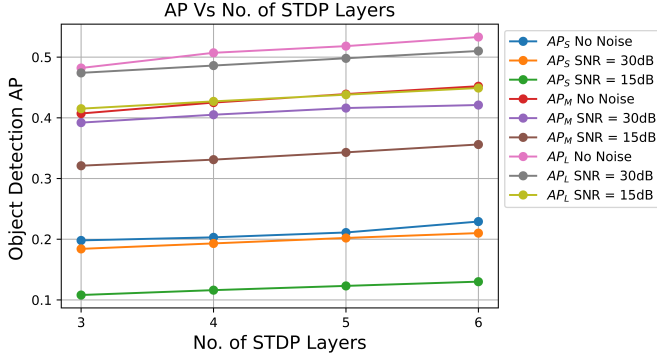


Fig. 8: Figure showing the change of small, medium and large object detection AP with increasing number of STDP layers

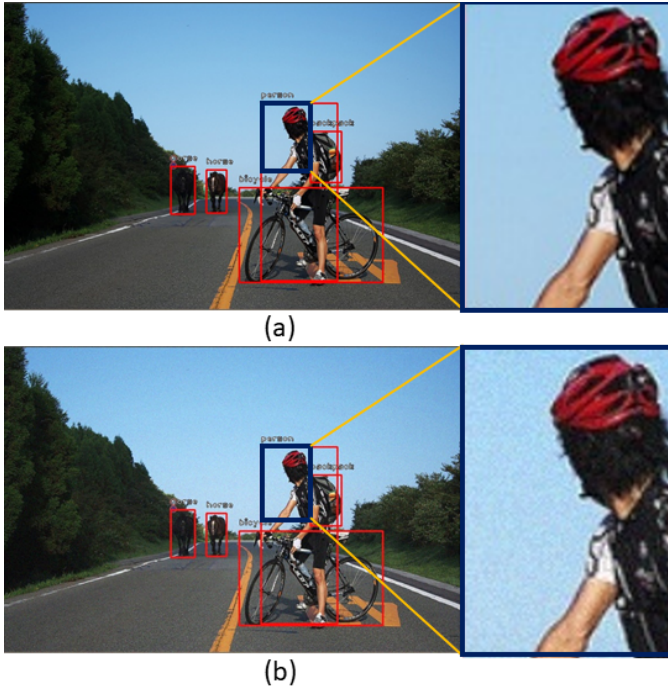


Fig. 9: FSHNN object detector performance on (a) clean and (b) noisy image with added Gaussian Noise and SNR = 15dB number of labeled training data.

2) Performance after Training with Less Labeled Data

To further demonstrate the robustness of the FSHNN object detector, we evaluated it with restrained training. We trained the model on a partial MS COCO dataset and reported the average precision and recall. We see that the object detectors with more STDP layers perform better especially when significant amounts of data are removed during training. Thus, we may conclude that the STDP layers trained with unlabeled data learn critical features for classification as can be seen from the

decrease in classification loss with increasing STDP layers in Table V. To get the confidence interval of the predictions in presence of noise, we tested the trained model 5 times. The mean and variance of the mAP are shown in Table X. For the case of limited training data, we performed a 3-fold cross-validation of the training subsets from the full COCO training set. The results reported are the mean and standard deviation of the mAX and the mean AX_S , AX_M , AX_L , mCMUE (where AX denotes AP or AR). We observe that the confidence interval is proportional to the mCMUE calculated. Also, it must be noted here that the change in the training data is for the backpropagated layers and not the STDP layers which are still trained on the full ImageNet traffic dataset as described before. However, the ImageNet traffic dataset used for training the STDP layers are unlabeled data and are thus much readily accessible compared to labeled data.

C. Comparison with Baselines

We compare the performance and energy efficiency of FSHNN with different baselines. The two baseline models for this comparison are described as follows (Table VI):

- *RetinaNet*: RetinaNet is a state-of-the-art DNN based object detector that works using the Focal Pyramid Network architecture. In this paper, we are using ResNet 101 as the backbone network for the RetinaNet object detector.
- *Back Propagated Fully Spiking Object Detector (BP-SOD)*: For the backpropagated fully spiking RetinaNet we replace the STDP layers (Block 1 in Fig. 1) in the FSHNN based object detector with corresponding DNN layers. For this experiment, we have replaced 3 STDP layers with 3 Convolution Layers. Hence, we use a similar DNN-to-SNN conversion methodology to obtain a Fully Spiking Object Detector with backpropagated spiking layers with the same architecture as FSHNN based object detector. With the weights obtained in this conversion process as the initialization point, we retrain the model using STBP to get the final trained model.

The parameters used for the RetinaNet and the BPSOD are summarized in Table VII.

1) Performance Comparison

We perform a two-fold evaluation of the FSHNN model with the baselines described above - first we evaluate the performance of the object detectors without any perturbation and train with the full training dataset. The results are represented in Table VIII. We see that the FSHNN with 6 STDP layers outperforms the RetinaNet with respect to both mAP/mAR and uncertainty error.

We test the robustness of the model by testing the model with different adversarial conditions - first, we use two different noise levels (SNR = 30dB, 15dB) and also evaluate the

TABLE V: Table showing Robustness of FSHNN based Object Detector for Noisy Testing Data and Limited Labeled Training Dataset

# STDP Layers	Class. Loss	Reg. Loss	mAP (mean±var)	mAR (mean±var)	mean mCMUE
SNR = 30dB					
3	0.4318	0.7165	0.366 ±0.00438	0.480 ±0.00473	0.317
4	0.3987	0.7093	0.379 ±0.00419	0.494 ±0.00466	0.305
5	0.3516	0.6845	0.392 ±0.00411	0.517 ±0.00462	0.291
6	0.3204	0.6522	0.412 ±0.00403	0.531 ±0.00452	0.284
SNR = 15dB					
3	0.6723	0.7345	0.302 ±0.00501	0.441 ±0.00522	0.455
4	0.6552	0.7269	0.316 ±0.00490	0.453 ±0.00513	0.448
5	0.6218	0.7114	0.321 ±0.00488	0.467 ±0.00511	0.439
6	0.6014	0.7008	0.330 ±0.00485	0.477 ±0.00503	0.431
80% of Labeled Training Data					
3	0.4157	0.6998	0.358 ±0.00453	0.475 ±0.00482	0.301
4	0.3806	0.6742	0.362 ±0.00450	0.480 ±0.00479	0.289
5	0.3694	0.6516	0.390 ±0.00445	0.513 ±0.00473	0.214
6	0.3356	0.6288	0.412 ±0.00439	0.547 ±0.00467	0.199
60% of Labeled Training Data					
3	0.4975	0.7884	0.329 ±0.00482	0.435 ±0.00501	0.390
4	0.4698	0.7545	0.341 ±0.00481	0.476 ±0.00497	0.358
5	0.4513	0.7312	0.364 ±0.00484	0.490 ±0.00499	0.317
6	0.4027	0.7084	0.391 ±0.00482	0.512 ±0.00496	0.296
40% of Labeled Training Data					
3	0.6057	0.9432	0.285 ±0.00520	0.385 ±0.00553	0.513
4	0.5964	0.9303	0.294 ±0.00516	0.400 ±0.00550	0.501
5	0.5837	0.9268	0.299 ±0.00511	0.415 ±0.00546	0.486
6	0.5759	0.9115	0.319 ±0.00504	0.423 ±0.00541	0.478

TABLE VI: Table Describing the Learning Blocks used in the Architectures

		Block 1	Block 2	ResNet Block	FPN Block
RetinaNet	Layer	None	None	DNN	DNN
	Learning	N/A	N/A	BP	BP
FSHNN Obj Det	Layer	SNN	SNN	SNN	SNN
	Learning	BP	STDP	BP	BP
BPSOD	Layer	SNN	SNN	SNN	SNN
	Learning	BP	BP	BP	BP

performance after training the model with increasingly limited labeled data (80%, 60%, and 40% data respectively).

We observe that in the no noise scenario, the FSHNN with 6 STDP layers outperforms the RetinaNet, and the difference in their performances increases as the input noise level is increased. Further, when the models are trained with a lesser amount of labeled data, even the FSHNN with 3 STDP layers perform better than the baseline ones.

TABLE VII: Table showing the hyperparameters used for the RetinaNet and BPSOD object detectors

RetinaNet Parameters	Value	BPSOD Parameters	Value
Batch Size	32	Batch Size	32
Epochs	100	Epochs	100
Backbone Size	ResNet-101	Max to Average Pooling	True
Optimizer	SGD	Spike Coding	Temporal Mean Rate
Learning Rate	0.001	MaxPool Type	Accumulated absolute spike rate [54]

In addition to this, we retrained and re-evaluated the models with varying conditions to get the confidence interval of the predictions as described in Sec. V-B2. We report the results for the mean and variance of mAX and the mean AX_S, AX_M, AX_L , mCMUE (where AX denotes AP or AR). The baseline performance of the model and the performance in presence of testing noise are shown in Tables VIII and IX respectively. The model's performance with limited training data is tabulated in Table X.

From Table VIII, we see that the FSHNN based object detector outperforms BPSOD. Thus, the use of STDP trained layers in the SNN shows a significant improvement in the mAP performance of the object detector compared to the backpropagated layers. This is because the STDP learning process extracts features that normal backpropagation-based feature extractors are unable to detect [46], [22], especially its ability to detect small objects as seen in Tables VIII, IX, X. Thus, the addition of STDP layers can be thought of as including a specialized addition of features that the BPSOD cannot capture and thus enhancing the performance. To empirically prove this, we evaluated the training loss of the BPSOD and the FSHNN object detectors. After 100 epochs, the FSHNN with 3-layer STDP had a training loss of 0.137, FSHNN with 6 STDP layers have a training loss of 0.129 and the BPSOD has a training loss of 0.162. Since the BPSOD has a higher training loss and also a higher testing loss, it shows that BPSOD is unable to extract features that the STDP based FSHNN can. The variation of training parameters does not lead to a huge variance in the observed mAP and the mAR of the BPSOD as can be seen in Table X. Thus, we can conclude that the BPSOD does not face the problem of converging to a local minima. Hence, we conclude that the FSHNN based model outperforms BPSOD because of better extraction of local features.

2) Generalizability of Object Proposal

As defined by Wang et. al, the generalizability of an object detector model is its ability to localize (not classify) unannotated objects in the training dataset [29]. For this experiment, we randomly split the MS-COCO dataset into two parts - the source dataset consisting of 70 seen classes and the target dataset of 10 unseen classes. We use the target dataset to evaluate the generalization of the proposal model trained with the source dataset. The train split is utilized for training and the 5000 images from the validation set during evaluation.

To evaluate the quality of the proposals, we use the standard average recall (AR@k) [55]. One of the primary motivations for building a generalized proposal model is to use the

TABLE VIII: Table showing the performance of the different object detectors

	mAP	AP _S	AP _M	AP _L	mAR	AR _S	AR _M	AR _L	mCMUE
No Noise; 100% Training Data									
RetinaNet	0.388	0.207	0.420	0.498	0.501	0.301	0.566	0.624	0.237
BPSOD	0.375	0.189	0.401	0.477	0.486	0.283	0.549	0.598	0.254
FSHNN Obj Det (6 STDP layers)	0.426	0.223	0.452	0.526	0.541	0.312	0.611	0.682	0.229

TABLE IX: Table showing the performance of the different object detectors with input noise during testing

	mAP (mean±var)	AP _S	AP _M	AP _L	mAR (mean±var)	AR _S	AR _M	AR _L	mean mCMUE
SNR = 30dB									
RetinaNet	0.372 ±0.00419	0.183	0.409	0.481	0.489 ±0.00439	0.279	0.554	0.613	0.313
BPSOD	0.363 ±0.00425	0.186	0.388	0.472	0.475 ±0.00443	0.278	0.543	0.589	0.320
FSHNN Obj Det (6 STDP layers)	0.409 ±0.00409	0.211	0.446	0.482	0.528 ±0.00430	0.308	0.599	0.668	0.284
SNR = 15dB									
RetinaNet	0.274 ±0.00611	0.104	0.237	0.349	0.412 ±0.00630	0.204	0.401	0.426	0.605
BPSOD	0.288 ±0.00605	0.159	0.347	0.406	0.419 ±0.00623	0.248	0.473	0.539	0.483
FSHNN Obj Det (6 STDP layers)	0.328 ±0.00501	0.184	0.392	0.451	0.474 ±0.00527	0.271	0.528	0.587	0.431

TABLE X: Table showing the performance of the different object detectors with different amount of labeled data

	mAP (mean±var)	AP _S	AP _M	AP _L	mAR (mean±var)	AR _S	AR _M	AR _L	mean mCMUE
80% of Labeled training set									
RetinaNet	0.369 ±0.00423	0.189	0.398	0.478	0.480 ±0.00435	0.287	0.543	0.608	0.308
BPSOD	0.349 ±0.00416	0.178	0.379	0.460	0.465 ±0.00456	0.264	0.525	0.574	0.305
FSHNN Obj Det (6 STDP layers)	0.408 ±0.00401	0.221	0.452	0.521	0.542 ±0.00421	0.311	0.594	0.662	0.199
60% of Labeled training set									
RetinaNet	0.322 ±0.00488	0.137	0.342	0.431	0.431 ±0.00515	0.231	0.492	0.557	0.393
BPSOD	0.313 ±0.00427	0.129	0.328	0.424	0.420 ±0.00469	0.221	0.476	0.541	0.396
FSHNN Obj Det (6 STDP layers)	0.392 ±0.00402	0.188	0.409	0.496	0.518 ±0.00436	0.271	0.542	0.608	0.296
40% of Labeled training set									
RetinaNet	0.236 ±0.00653	0.056	0.266	0.351	0.345 ±0.00679	0.158	0.413	0.472	0.799
BPSOD	0.251 ±0.00617	0.076	0.262	0.368	0.362 ±0.00632	0.163	0.412	0.487	0.613
FSHNN Obj Det (6 STDP layers)	0.319 ±0.00506	0.126	0.337	0.439	0.421 ±0.00529	0.221	0.492	0.553	0.478

resulting proposals to train detection models for unseen classes with limited or no bounding box annotation.

We compare the generalization ability of the FSHNN based object detector and RetinaNet in Table. XI. The models are trained on the COCO-source-train dataset as described above. We report AR@100 on seen classes in the COCO-source-test dataset and unseen classes in the COCO-target-test. We build on the hypothesis that the difference in performance between seen and unseen classes reflects the generalization gap. We also show an upper-bound performance on COCO-target-test obtained by models trained on the full training dataset containing both COCO-source-train and COCO-target-train. On seen classes, RetinaNet achieves a worse performance compared to FSHNN (a drop of 7.01%). However, the drop is larger for unseen target classes (a drop of 11.9%), indicating a larger generalization gap for RetinaNet. One reason for this is that RetinaNet is more sensitive to missing bounding boxes corresponding to unlabeled unseen classes in the source dataset. Also, since RetinaNet uses focal-loss, the unseen and unannotated object classes proposals in the training data are treated as hard-negatives. Thus, the model heavily penalizes

proposals corresponding to unannotated bounding boxes, leading to an overall decrease in AR. Since some seen classes share visual similarities with unseen classes, this sensitivity to missing annotations also affects AR for seen classes. However, this effect is more magnified for unseen target classes. On the other hand, in FSHNN, only a small number of proposals that do not intersect with annotated bounding boxes are sampled at random as negatives. Hence, the probability that a proposal corresponding to an unseen object class is negative is lower, leading to better generalization. Thus, we observe that the detection head of FSHNN provides better overall performance without sacrificing generalization.

D. Comparison with other Hybrid Models

In this section, we compare the performance of the FSHNN based object detectors with other hybrid models. To do so, we replace the STDP based Spiking CNN layers (Block 2) shown in Fig. 1 with other unsupervised feature extractors and evaluated the new object detectors obtained on the MS-COCO dataset similar to the FSHNN model. It is to be noted here that the rest of the models are the same as FSHNN i.e., they are trained with a DNN-to-SNN conversion followed by

TABLE XI: AR@100 corresponding to different baseline models trained on COCO-source-train and evaluated on different test splits. Upper-bound corresponds to model trained on full COCO dataset and evaluated on COCO-target-test.

	COCO-source-test	COCO-target-test
RetinaNet	55.7	41.5
BPSOD	51.8	39.9
FSHNN Obj Det (3 STDP Layers)	55.7	47.9
FSHNN Obj Det (6 STDP Layers)	56.2	48.4

a STDB finetuning, as shown in Fig. 7. Also, it is to be noted here that the unsupervised models mentioned here are based on DNNs and not converted to SNNs using conversion techniques. The features extracted using these methods are then converted into spikes using a Difference of Gaussian (DoG) filter [22] which generates a spike train detecting the positive or negative contrasts in the feature space. The output of the DoG filter is fed into the spiking ResNet block after concatenating with the spiking output of Block 1. The unsupervised models used for the comparison are listed as follows:

- **Unsupervised Convolutional Siamese Network (UCSN)** : We use an Unsupervised Convolutional Siamese Network for feature extraction [56]. It is a new deep learning-based feature extractor consisting of an end-to-end trained convolutional neural network for adaptive neighborhood embedding in an unsupervised manner. In this experiment, we use the UCSN-HOG which uses the distance between the Histogram of Oriented Gradients (HOG) features which is a type of global image descriptor.
- **Convolutional Autoencoder (CAE)**: They are a type of Convolutional Neural Networks (CNNs) that are trained only to learn filters able to extract features that can be used to reconstruct the input. CNNs are usually referred to as supervised learning algorithms. The latter, instead, are trained only to learn filters able to extract features that can be used to reconstruct the input. Each CAE is trained using conventional online gradient descent without additional regularization terms. For the simulation, we initialized a convolutional neural network (CNN) with trained convolutional auto-encoder weights as described by Masci et al. [57].

The detailed block architecture are summarized in Table XII and the results are shown in Table XIII. We see that the FSHNN based object detector outperforms the other DNN based hybrid learning models, especially in small object detection.

Generalizability of Hybrid Networks: Similarly, we also check the generalizability of the other hybrid models discussed above. We evaluate these hybrid models on the COCO-source-test and the COCO-target-test datasets and reported their AR@100 scores in Table XIV. We see that the generalizability of object proposals of the FSHNN based object detector is better than the DNN based unsupervised hybrid models. This shows that STDP based feature extractors generalize better than alternative unsupervised learning models for DNN.

TABLE XII: Table Describing the Learning Blocks used in the **Other Hybrid Learning Architectures** for Object Detection

		Block 1	Block 2	ResNet Block	FPN Block
Hybrid UCSN Obj Det	Layer	SNN	DNN	SNN	SNN
	Learning	BP	UCSN	BP	BP
Hybrid CAE Obj Det	Layer	SNN	DNN	SNN	SNN
	Learning	BP	CAE	BP	BP

E. Ablation Studies

We consider the ablation studies of the FSHNN object detector discussed before.

The three types of ablation network studied in this section are described as follows:

- **STDP-STDP Spiking Object Detector:** This object detector is made using a 4-layer STDP trained SNN block in place of the Backpropagated SCNN module (Block 1 in Fig. 1) in addition to the STDP SCNN module (Block 2 in Fig. 1)
- **Null-STDP Spiking Object Detector:** This ablation network is obtained by removing the BP SCNN module (Block 1) from the FSHNN model and adding only the STDP SCNN module (Block 2) to the Spiking RetinaNet model.
- **BP-Null Spiking Object Detector:** For this ablation study, we remove the STDP SCNN module (Block 2) from the FSHNN model and only keep the BP SCNN module (Block 1).

We evaluate the performance of these ablation networks on the MS-COCO dataset. The detailed block architecture is summarized in Table XV and the results are shown in Table XVI. We see that the FSHNN object detector outperforms the other ablation networks. This ablation study also proves that the sole usage of either STDP based layers or back-propagated spiking layers cannot extract the features which a hybrid method can.

Generalizability of Ablation Networks: Similarly, we also check the generalizability of the ablation networks discussed above. We also evaluate these ablation models on the COCO-source-test and the COCO-target-test datasets and evaluated their AR@100 scores. The results are also shown in Table XVII. We see that the generalizability of object proposals of the FSHNN based object detector is better than the ablation networks. The results show that though the STDP-STDP performs poorly, it has the least dip in the source-to-target translation (a drop of 22.5% in comparison to 24.4% in Null-STDP and 33% in BP-Null). This shows that STDP layers help generalize better object proposals

F. Energy Efficiency Comparison

We next compare the energy advantage of spiking models (FSHNN and Backpropagated spiking layer) with RetinaNet (Table XVIII). As discussed by Kim et al. [10], most operations in DNNs occur in convolutional layers where the multiply-accumulate (MAC) operations are primarily responsible during execution. However, SNNs perform accumulate (AC) operations because spike events are binary operations whose input is integrated into a membrane potential only when spikes are received. Thus, SNNs save computational energy due to the use of AC instead of operations in SNNs.

TABLE XIII: Table showing Performance Comparison of Object Detectors based on **other Hybrid Models**

Number of STDP Layers	mAP	AP _S	AP _M	AP _L	mAR	AR _S	AR _M	AR _L
FSHNN Obj Det (6 STDP Layers)	0.426	0.229	0.452	0.533	0.541	0.327	0.612	0.668
Hybrid UCSN Obj Det	0.383	0.191	0.411	0.487	0.497	0.290	0.559	0.621
Hybrid UCSN CAE Det	0.381	0.189	0.415	0.486	0.500	0.289	0.561	0.627

TABLE XIV: AR@100 corresponding to different hybrid models trained on COCO-source-train and evaluated on different test splits.

	COCO-source-test	COCO-target-test
Hybrid UCSN Obj Det	51.8	36.7
Hybrid CAE Obj Det	51.4	36.4
FSHNN Obj Det (6 STDP Layers)	56.2	48.4

TABLE XV: Table Describing the Learning Blocks used in the Architectures for **Ablation Studies**

		Block 1	Block 2	ResNet Block	FPN Block
STDP-STDP Spiking Obj Det	Layer	SNN	SNN	SNN	SNN
	Learning	STDP	STDP	BP	BP
Null-STDP Spiking Obj Det	Layer	None	SNN	SNN	SNN
	Learning	N/A	STDP	BP	BP
BP-Null Spiking Obj Det	Layer	SNN	None	SNN	SNN
	Learning	BP	N/A	BP	BP
FSHNN Obj Det	Layer	SNN	SNN	SNN	SNN
	Learning	BP	STDP	BP	BP

The number of parameters vs MACs/ACs for the different architectures are summarized in Table XVIII.

Horowitz et. al. [58] showed that in an in 45nm 0.9V chip, a 32-bit floating-point (FL) MAC operation consumes 4.6 pJ and 0.9 pJ for an AC operation. Based on these measures, we calculated the energy consumption of the spiking object detectors by multiplying FLOPS (floating-point operations) and the energy consumption of MAC and AC operations calculated. A simplified estimate of the computational energy E for ANN/SNN considering FLOPS count across all N layers of a network can be obtained as [2]:

$$E_{ANN} = \left(\sum_{i=1}^N FLOPS_{ANN} \right) * E_{MAC} \quad (9)$$

$$E_{SNN} = \left(\sum_{i=1}^N FLOPS_{SNN} \right) * E_{AC} * T$$

For SNN, the energy calculation considers the latency incurred as the rate-coded input spike train has to be presented over T time-steps to yield the final prediction result. Since we are using a training methodology using STDB [11] which takes much fewer timesteps, we have considered the number of time steps $T = 300$.

It should be noted that the prior analysis only considers computational energy savings. More detailed analysis is necessary to understand the total energy advantage of SNN over ANN considering various hardware design issues. For example, neuromorphic hardware that uses event-driven computing consumes only static power in the absence of spikes. On the other hand, clock-driven designs benefit much less from sparsity. Also, even on an event-driven neuromorphic chip, there is an additional cost when using spiking neurons - since the neurons must maintain state values over time

unlike DNNs which are state-less, their potential needs to be stored, which has an important memory footprint. Further, membrane potential of the neurons must be updated multiple times (once for every time steps) while evaluating an image thereby incurring additional memory read and write energy dissipations. All of the above factors must be considered for a more accurate analysis of energy advantage of SNN. However, as the focus of this paper is developing the hybrid learning model for object detection, such detailed energy analysis is beyond the scope of this paper.

G. Comparison to Spiking Yolo

We compare FSHNN model performance with the state-of-art spike-based object detector - Spiking YOLO [10]. Though both of them are fully spiking object detectors, there are a few key differences between the two. First, the Spiking Yolo is composed of backpropagated Spiking Convolution Layers that are trained using supervised learning. In contrast, FSHNN couples both STDP based unsupervised learning methodologies with backpropagation learning. This helps the FSHNN network achieve high performance as well as robustness against input noise and less labeled data for training. Second, we analyze the uncertainty and generalizability properties of FSHNN; but such analyses were not performed for spiking YOLO[10]. Third, FSHNN shows a higher performance than spiking YOLO. While the spiking YOLO reported an mAP of 26.24% [10], the FSHNN network with 6 STDP layers described in this paper achieves an mAP of 42.6%. We note that the spiking YOLO object detector is based on the YOLO architecture. The YOLO architecture suffers from an extreme class imbalance where the detectors evaluate a lot of extra candidate locations a majority of which do not contain an object. In contrast, FSHNN uses the RetinaNet architecture that fixes this issue by using the Focal Pyramid Network and the Focal Loss. The Spiking YOLO is based on the Tiny YOLO object detector architecture which uses 6.97×10^9 FLOPS of computation. On the other hand, the channel-norm-based spiking YOLO uses 4.9×10^7 FLOPS of computation in 3500 time steps. Thus the theoretical energy efficiency achieved using the Spiking YOLO compared to the tiny YOLO is only 1.4x. It must be noted here that the proposed FSHNN based object detectors use almost 4x the number of FLOPS. However, the use of the STDB method greatly reduces the time steps needed from 3500 to just 300 as used in this paper. This leads to a huge difference in energy efficiency in the two models.

VI. CONCLUSION

We have presented fully spiking hybrid neural network (FSHNN), a novel spiking neural network based object detector by fusing features extracted from both unsupervised STDP

TABLE XVI: Table showing Performance Comparison of the Architectures in Ablation Studies

Number of STDP Layers	mAP	AP _S	AP _M	AP _L	mAR	AR _S	AR _M	AR _L
6 layer STDP FSHNN	0.426	0.229	0.452	0.533	0.541	0.327	0.612	0.668
STDP-STDP Spiking Obj Det	0.268	0.119	0.284	0.356	0.376	0.195	0.396	0.489
Null-STDP Spiking Obj Det	0.251	0.106	0.279	0.348	0.369	0.190	0.387	0.481
BP-Null Spiking Obj Det	0.315	0.155	0.342	0.416	0.423	0.215	0.480	0.512

TABLE XVII: AR@100 corresponding to different ablation models trained on COCO-source-train and evaluated on different test splits.

	COCO-source-test	COCO-target-test
STDP-STDP Spiking Obj Det	42.5	32.9
Null-STDP Spiking Obj Det	41.8	31.6
BP-Null Spiking Obj Det	50.5	33.5
FSHNN Obj Det (6 STDP Layers)	56.2	48.4

TABLE XVIII: Table showing the energy efficiency of object detectors based on SNNs

	Param(M)	MACs/ ACs	$EE = \frac{EE_{ANN}}{EE_{SNN}}$
RetinaNet	52.78	MAC: 131.41×10^9	N/A
BPSOD	52.99	AC: 9.2×10^7	151.53
FSHNN Obj Det (3 layers STDP)	52.96	AC: 9.1×10^7	154.88
FSHNN Obj Det (6 layers STDP)	53.11	AC: 9.5×10^7	147.54

based learning and supervised backpropagation based learning. We have also developed used a MC dropout based sampling method to estimate the uncertainty of FSHNN. Experimental results on MSCOCO dataset shows that the FSHNN demonstrates comparable or better performance than standard DNN while promising orders of magnitude improvement in energy-efficiency. Further, we have observed that FSHNN network outperforms the baseline DNN as well as a spiking network trained with backpropagation when tested under input noise or trained with less available labelled data. We have also shown that integration of STDP learning helps improve generalization ability of FSHNN. In conclusion, we demonstrated the feasibility of designing a fully spiking network for object detection facilitating the deployment spiking networks for resource-constrained environments.

REFERENCES

- [1] W. Maass, "Networks of spiking neurons: the third generation of neural network models," *Neural networks*, vol. 10, no. 9, pp. 1659–1671, 1997.
- [2] P. Panda, S. A. Aketi, and K. Roy, "Toward scalable, efficient, and accurate deep spiking neural networks with backward residual connections, stochastic softmax, and hybridization," *Frontiers in Neuroscience*, vol. 14, 2020.
- [3] J. V. Stone, "Principles of neural information theory," *Computational Neuroscience and Metabolic Efficiency*, 2018.
- [4] P. A. Merolla, J. V. Arthur, R. Alvarez-Icaza, A. S. Cassidy, J. Sawada, F. Akopyan, B. L. Jackson, N. Imam, C. Guo, Y. Nakamura *et al.*, "A million spiking-neuron integrated circuit with a scalable communication network and interface," *Science*, vol. 345, no. 6197, pp. 668–673, 2014.
- [5] S. Carrillo, J. Harkin, L. McDaid, S. Pande, S. Cawley, B. McGinley, and F. Morgan, "Advancing interconnect density for spiking neural network hardware implementations using traffic-aware adaptive network-on-chip routers," *Neural networks*, vol. 33, pp. 42–57, 2012.
- [6] T. V. Bliss and G. L. Collingridge, "A synaptic model of memory: long-term potentiation in the hippocampus," *Nature*, vol. 361, no. 6407, pp. 31–39, 1993.
- [7] A. Tavanaei and A. S. Maida, "Bio-inspired spiking convolutional neural network using layer-wise sparse coding and stdp learning," *arXiv preprint arXiv:1611.03000*, 2016.
- [8] P. Panda and N. Srinivasa, "Learning to recognize actions from limited training examples using a recurrent spiking neural model," *Frontiers in neuroscience*, vol. 12, p. 126, 2018.
- [9] J. Deng, W. Dong, R. Socher, L.-J. Li, K. Li, and L. Fei-Fei, "Imagenet: A large-scale hierarchical image database," in *2009 IEEE conference on computer vision and pattern recognition*. Ieee, 2009, pp. 248–255.
- [10] S. Kim, S. Park, B. Na, and S. Yoon, "Spiking-yolo: Spiking neural network for energy-efficient object detection," in *Proceedings of the AAAI Conference on Artificial Intelligence*, vol. 34, no. 07, 2020, pp. 11 270–11 277.
- [11] N. Rathi, G. Srinivasan, P. Panda, and K. Roy, "Enabling deep spiking neural networks with hybrid conversion and spike timing dependent backpropagation," *arXiv preprint arXiv:2005.01807*, 2020.
- [12] B. Nessler, M. Pfeiffer, L. Buesing, and W. Maass, "Bayesian computation emerges in generic cortical microcircuits through spike-timing-dependent plasticity," *PLoS Comput Biol*, vol. 9, no. 4, p. e1003037, 2013.
- [13] W. Liu, D. Anguelov, D. Erhan, C. Szegedy, S. Reed, C.-Y. Fu, and A. C. Berg, "Ssd: Single shot multibox detector," in *European conference on computer vision*. Springer, 2016, pp. 21–37.
- [14] J. Redmon and A. Farhadi, "Yolov3: An incremental improvement," *arXiv preprint arXiv:1804.02767*, 2018.
- [15] T.-Y. Lin, P. Goyal, R. Girshick, K. He, and P. Dollár, "Focal loss for dense object detection," in *Proceedings of the IEEE international conference on computer vision*, 2017, pp. 2980–2988.
- [16] A. Sengupta, Y. Ye, R. Wang, C. Liu, and K. Roy, "Going deeper in spiking neural networks: Vgg and residual architectures," *Frontiers in neuroscience*, vol. 13, p. 95, 2019.
- [17] P. U. Diehl, D. Neil, J. Binas, M. Cook, S.-C. Liu, and M. Pfeiffer, "Fast-classifying, high-accuracy spiking deep networks through weight and threshold balancing," in *2015 International joint conference on neural networks (IJCNN)*. IEEE, 2015, pp. 1–8.
- [18] B. Rueckauer, I.-A. Lungu, Y. Hu, and M. Pfeiffer, "Theory and tools for the conversion of analog to spiking convolutional neural networks," *arXiv preprint arXiv:1612.04052*, 2016.
- [19] J. R. Miquel, S. Tolu, F. E. Schöller, and R. Galeazzi, "Retinanet object detector based on analog-to-spiking neural network conversion," *arXiv preprint arXiv:2106.05624*, 2021.
- [20] S. Huang, C. Rozas, M. Trevino, J. Contreras, S. Yang, L. Song, T. Yoshioka, H.-K. Lee, and A. Kirkwood, "Associative hebbian synaptic plasticity in primate visual cortex," *Journal of Neuroscience*, vol. 34, no. 22, pp. 7575–7579, 2014.
- [21] P. U. Diehl, G. Zarella, A. Cassidy, B. U. Pedroni, and E. Neftci, "Conversion of artificial recurrent neural networks to spiking neural networks for low-power neuromorphic hardware," in *2016 IEEE International Conference on Rebooting Computing (ICRC)*. IEEE, 2016, pp. 1–8.
- [22] S. R. Kheradpisheh, M. Ganjtabesh, S. J. Thorpe, and T. Masquelier, "Stdp-based spiking deep convolutional neural networks for object recognition," *Neural Networks*, vol. 99, pp. 56–67, 2018.
- [23] Y. Wu, L. Deng, G. Li, J. Zhu, and L. Shi, "Spatio-temporal backpropagation for training high-performance spiking neural networks," *Frontiers in neuroscience*, vol. 12, p. 331, 2018.
- [24] A. Jacot, F. Gabriel, and C. Hongler, "Neural tangent kernel: Convergence and generalization in neural networks," in *Advances in neural information processing systems*, 2018, pp. 8571–8580.

- [25] K. Huang, Y. Wang, M. Tao, and T. Zhao, "Why do deep residual networks generalize better than deep feedforward networks?—a neural tangent kernel perspective," *arXiv preprint arXiv:2002.06262*, 2020.
- [26] Z. Chen, Y. Cao, Q. Gu, and T. Zhang, "A generalized neural tangent kernel analysis for two-layer neural networks," *Advances in Neural Information Processing Systems*, vol. 33, 2020.
- [27] U. Şimşekli, O. Sener, G. Deligiannidis, and M. A. Erdogdu, "Hausdorff dimension, stochastic differential equations, and generalization in neural networks," *arXiv preprint arXiv:2006.09313*, 2020.
- [28] M. Gurbuzbalaban, U. Simsekli, and L. Zhu, "The heavy-tail phenomenon in sgd," *arXiv preprint arXiv:2006.04740*, 2020.
- [29] R. Wang, D. Mahajan, and V. Ramanathan, "What leads to generalization of object proposals?" *arXiv preprint arXiv:2008.05700*, 2020.
- [30] R. Moreno-Bote and J. Drugowitsch, "Causal inference and explaining away in a spiking network," *Scientific reports*, vol. 5, no. 1, pp. 1–18, 2015.
- [31] B. J. Lansdell and K. P. Kording, "Spiking allows neurons to estimate their causal effect," *bioRxiv*, p. 253351, 2018.
- [32] T. V. Bliss and T. Lomo, "Long-lasting potentiation of synaptic transmission in the dentate area of the anaesthetized rabbit following stimulation of the perforant path," *The Journal of physiology*, vol. 232, no. 2, pp. 331–356, 1973.
- [33] W. Gerstner, R. Ritz, and J. L. Van Hemmen, "Why spikes? hebbian learning and retrieval of time-resolved excitation patterns," *Biological cybernetics*, vol. 69, no. 5, pp. 503–515, 1993.
- [34] M. D. Zeiler and R. Fergus, "Visualizing and understanding convolutional networks," in *European conference on computer vision*. Springer, 2014, pp. 818–833.
- [35] J. Donahue, Y. Jia, O. Vinyals, J. Hoffman, N. Zhang, E. Tzeng, and T. Darrell, "Decaf: A deep convolutional activation feature for generic visual recognition," in *International conference on machine learning*, 2014, pp. 647–655.
- [36] J. Yosinski, J. Clune, Y. Bengio, and H. Lipson, "How transferable are features in deep neural networks?" in *Advances in neural information processing systems*, 2014, pp. 3320–3328.
- [37] T. K. Leen, R. Friel, and D. Nielsen, "Approximating distributions in stochastic learning," *Neural networks*, vol. 32, pp. 219–228, 2012.
- [38] U. Simsekli, O. Sener, G. Deligiannidis, and M. A. Erdogdu, "Hausdorff dimension, heavy tails, and generalization in neural networks," *Advances in Neural Information Processing Systems*, vol. 33, 2020.
- [39] D. Kappel, S. Habenschuss, R. Legenstein, and W. Maass, "Synaptic sampling: A bayesian approach to neural network plasticity and rewiring," in *Advances in Neural Information Processing Systems*, 2015, pp. 370–378.
- [40] U. Simsekli, L. Sagun, and M. Gurbuzbalaban, "A tail-index analysis of stochastic gradient noise in deep neural networks," *arXiv preprint arXiv:1901.06053*, 2019.
- [41] B. M. Hill, "A simple general approach to inference about the tail of a distribution," *The annals of statistics*, pp. 1163–1174, 1975.
- [42] J. Pickands III *et al.*, "Statistical inference using extreme order statistics," *the Annals of Statistics*, vol. 3, no. 1, pp. 119–131, 1975.
- [43] S. Mittnik and S. T. Rachev, "Tail estimation of the stable index α ," *Applied Mathematics Letters*, vol. 9, no. 3, pp. 53–56, 1996.
- [44] V. Paulauskas and M. Vaičiulis, "Once more on comparison of tail index estimators," *arXiv preprint arXiv:1104.1242*, 2011.
- [45] M. Mohammadi, A. Mohammadpour, and H. Ogata, "On estimating the tail index and the spectral measure of multivariate α -stable distributions," *Metrika*, vol. 78, no. 5, pp. 549–561, 2015.
- [46] X. She, P. Saha, D. Kim, Y. Long, and S. Mukhopadhyay, "Safe-dnn: A deep neural network with spike assisted feature extraction for noise robust inference," in *2020 International Joint Conference on Neural Networks (IJCNN)*. IEEE, 2020, pp. 1–8.
- [47] A. Tavanaei, M. Ghodrati, S. R. Kheradpisheh, T. Masquelier, and A. Maida, "Deep learning in spiking neural networks," *Neural Networks*, vol. 111, pp. 47–63, 2019.
- [48] B. Rueckauer, I.-A. Lungu, Y. Hu, M. Pfeiffer, and S.-C. Liu, "Conversion of continuous-valued deep networks to efficient event-driven networks for image classification," *Frontiers in neuroscience*, vol. 11, p. 682, 2017.
- [49] Y. Gal and Z. Ghahramani, "Dropout as a bayesian approximation: Representing model uncertainty in deep learning," in *international conference on machine learning*, 2016, pp. 1050–1059.
- [50] C. Lee, S. S. Sarwar, P. Panda, G. Srinivasan, and K. Roy, "Enabling spike-based backpropagation for training deep neural network architectures," *Frontiers in Neuroscience*, vol. 14, 2020.
- [51] D. Miller, L. Nicholson, F. Dayoub, and N. Sünderhauf, "Dropout sampling for robust object detection in open-set conditions," in *2018 IEEE International Conference on Robotics and Automation (ICRA)*. IEEE, 2018, pp. 1–7.
- [52] T.-Y. Lin, M. Maire, S. Belongie, J. Hays, P. Perona, D. Ramanan, P. Dollár, and C. L. Zitnick, "Microsoft coco: Common objects in context," in *European conference on computer vision*. Springer, 2014, pp. 740–755.
- [53] D. Miller, F. Dayoub, M. Milford, and N. Sünderhauf, "Evaluating merging strategies for sampling-based uncertainty techniques in object detection," in *2019 International Conference on Robotics and Automation (ICRA)*. IEEE, 2019, pp. 2348–2354.
- [54] Y. Hu and M. Pfeiffer, "Max-pooling operations in deep spiking neural networks," 2016.
- [55] J. Hosang, R. Benenson, P. Dollár, and B. Schiele, "What makes for effective detection proposals?" *IEEE transactions on pattern analysis and machine intelligence*, vol. 38, no. 4, pp. 814–830, 2015.
- [56] D. J. Trosten and P. Sharma, "Unsupervised feature extraction—a cnn-based approach," in *Scandinavian Conference on Image Analysis*. Springer, 2019, pp. 197–208.
- [57] J. Masci, U. Meier, D. Cireşan, and J. Schmidhuber, "Stacked convolutional auto-encoders for hierarchical feature extraction," in *International conference on artificial neural networks*. Springer, 2011, pp. 52–59.
- [58] M. Horowitz, "1.1 computing's energy problem (and what we can do about it)," in 2014 IEEE International Solid-State Circuits Conference Digest of Technical Papers (ISSCC), in *IEEE, feb*, 2014.